

Blind and non-blind source detection in WMAP 5-year maps

M. Massardi^{1,2*}, M. López-Caniego³, J. González-Nuevo¹, D. Herranz⁴,
G. De Zotti^{5,1}, and J. L. Sanz^{4,6}

¹ *SISSA-I.S.A.S, via Beirut 4, I-34014 Trieste, Italy*

² *Australia Telescope National Facility, CSIRO, PO Box 76 Epping, NSW 1710, Australia*

³ *Astrophysics Group, Cavendish Laboratory, J.J. Thomson Avenue, CB3 0E1, Cambridge, United Kingdom*

⁴ *Instituto de Física de Cantabria (CSIC-UC), Avda. los Castros s/n, 39005 Santander, Spain*

⁵ *INAF-Osservatorio Astronomico di Padova, vicolo dell'Osservatorio 5, I-35122 Padova, Italy*

⁶ *CNR Istituto di Scienza e Tecnologie dell'Informazione, I-56124, Pisa, Italy*

1 November 2018

ABSTRACT

We have analyzed the efficiency in source detection and flux density estimation of *blind* and *non-blind* detection techniques exploiting the MHW2 filter applied to the Wilkinson Microwave Anisotropy Probe (WMAP) 5-year maps. A comparison with the AT20G Bright Source Sample (Massardi et al. 2008), with a completeness limit of 0.5 Jy and accurate flux measurements at 20 GHz, close to the lowest frequency of WMAP maps, has allowed us to assess the completeness and the reliability of the samples detected with the two approaches, as well as the accuracy of flux and error estimates, and their variations across the sky. The uncertainties on flux estimates given by our procedure turned out to be about a factor of 2 lower than the rms differences with AT20G measurements, consistent with the smoothing of the fluctuation field yielded by map filtering. Flux estimates were found to be essentially unbiased except that, close to the detection limit, a substantial fraction of fluxes are found to be inflated by the contribution of underlying positive fluctuations. This is consistent with expectations for the Eddington bias associated to the true errors on flux density estimates. The blind and non-blind approaches are found to be complementary: each of them allows the detection of sources missed by the other. Combining results of the two methods on the WMAP 5-year maps we have expanded the non-blindly generated New Extragalactic WMAP Point Source (NEWPS) catalogue (López-Caniego et al. 2007) that was based on WMAP 3-year maps. After having removed the probably spurious objects not identified with known radio sources, the new version of the NEWPS catalogue, NEWPS_5yr comprises 484 sources detected with a signal-to-noise ratio $\text{SNR} \geq 5$.

Key words: surveys – galaxies: active – cosmic microwave background – radio continuum: galaxies – radio continuum: general.

1 INTRODUCTION

The best spectral region to study the Cosmic Microwave Background (CMB) is the millimetric wavelength band, where the overall contamination from foregrounds is at a minimum and the CMB black body spectrum is close to its peak. An important byproduct of CMB experiments is information on point sources, whose millimeter-wave properties are poorly known. On the other hand, a careful extraction of

point sources from CMB maps is crucial since they are the main foreground contaminant on small angular scales (less than $\sim 30'$; De Zotti et al. 1999; Toffolatti et al. 1999).

The WMAP mission has produced the first all-sky surveys of extragalactic sources at 23, 33, 41, 61 and 94 GHz. The analysis of first year data yielded a sample of 208 extragalactic sources detected above a flux limit of ~ 0.8 -1 Jy (Bennett et al. 2003), with an estimated completeness limit of ~ 1.2 Jy at 23 GHz (Argüeso et al. 2003; De Zotti et al. 2005). The sample size has been steadily increasing as the WMAP survey successfully progressed: 323 sources were

* E-mail: massardi@sissa.it

found in the 3-yr maps (Hinshaw et al. 2007; we will refer to this sample as WMAP_3yr), and 390 in the 5-yr maps (Wright et al. 2008; WMAP_5yr sample). The approach used by the WMAP team for source extraction can be summarized as follows. The temperature map pixels were first weighted by $N_{\text{obs}}^{1/2}$, N_{obs} being the number of independent observations per pixel, and then filtered in harmonic space by the global matched filter $b_l/(b_l^2 C_l^{\text{CMB}} + C_l^{\text{noise}})$, where b_l is the transfer function of the WMAP beam response, C_l^{CMB} is the CMB angular power spectrum, and C_l^{noise} is the noise power spectrum. Peaks with signal-to-noise ratio (SNR) greater than 5 (note that the ‘noise’ here is the global rms fluctuation in regions outside the processing mask) in any band were interpreted as source detections. The peaks are fitted in real space, i.e. in the unfiltered maps, to a Gaussian profile plus a planar baseline to estimate the flux densities. The flux densities in the other channels are given if their SNR > 2 and the source width falls within a factor of two of the true beam width.

Several other attempts to improve the source detection have been presented. Nie & Zhang (2007) applied cross-correlation techniques to clean the WMAP first-year residual maps and identify foreground residuals which have been associated to radio sources: they detected 101 sources of which 26 were not in the WMAP 1-year catalogue (25 of them do not appear even in the WMAP_3yr catalogue, but 5 of them are in the LMC region). Chen & Wright (2008), combining the 61 and 94 GHz WMAP temperature maps to cancel the ‘noise’ due to the CMB anisotropy signal, found 31 sources in the first year maps and 64 in the 3-year co-added maps, of which 21 are not in WMAP_3yr. The same $V - W$ internal linear combination technique was used by Wright et al. (2008) to find 99 sources in the region with $|b| > 10^\circ$, 64 of which are in WMAP_5yr, 17 can be identified with known sources, 17 are in complex Galactic emission regions, and 1 is unidentified.

In previous works, we have used a non-blind approach (see López-Caniego et al. 2007, González-Nuevo et al. 2008, hereafter LC07 and GN08, respectively) exploiting the MHW2 filter (González-Nuevo et al. 2006) to obtain estimates of (or upper limits to) the flux densities at the WMAP frequencies for a complete all-sky sample of 2491 sources with $|b| > 5^\circ$, brighter than 500 mJy at 5 GHz in the PMN (Griffith et al. 1993, 1995; Wright et al. 1994, 1996) or in the GB6 (Gregory et al. 1996) catalogs, or at 1.4 or 0.84 GHz in regions not covered by 5 GHz surveys but covered by either the NVSS (Condon et al. 1998) or the SUMSS (Mauch et al. 2003, 2007). This work yielded 5σ detections of 380 extragalactic sources in the WMAP 3-yr maps, including 98 sources not present in the WMAP_3yr catalog. The results were organized in the NEWPS (New Extragalactic WMAP Point Source) catalog (since it is based on 3-year maps we will hereafter add the suffix ‘3yr’ to the name).

In this paper we extend the analysis to the WMAP 5-yr data, carrying out both a ‘blind’ and a ‘non-blind’ source search using the same filter (MHW2), that was shown by López-Caniego et al. (2006) to be essentially as efficient as the matched filter, and easier to use. A particularly delicate issue that we will address is the estimate of the ‘noise’ to be used to derive the SNR and hence the nominal flux limit for source detection, in the presence of a highly inhomogeneous fluctuation field. This analysis is important also in

view of defining the optimal source extraction strategy for the Planck mission.

The strong inhomogeneity and non-Gaussianity of the fluctuation field, which in the best CMB experiments is dominated not by the instrumental noise but by sources below the detection limit and by small-scale structure in the Galactic emission, is a serious hindrance for source detection techniques. Since the statistical properties of such fluctuation field are poorly known, the reliability of source detections and the real uncertainties on flux estimates are difficult to quantify, even in the case of relatively high SNR’s. It is well known (Eddington 1913; Murdoch et al. 1973; Hogg & Turner 1998) that the skewness of the distribution of Poisson fluctuations due to unresolved sources may strongly bias flux estimates with SNR < 5 , and the effect is larger for steeper source counts. Source clustering and small-scale structure of the Galactic emission may substantially worsen the problem for low resolution experiments, such as those aimed at mapping the CMB. Simulations of Planck observations (Leach et al. 2008) show that both the fraction of spurious detections and the incompleteness level may be of several percent, even at flux limits corresponding to SNR ≥ 5 .

Fortunately the Bright Source Sample (BSS; Massardi et al. 2008, M08 hereafter), complete down to $S_{20\text{GHz}} = 0.5\text{Jy}$ for $\delta < -15^\circ$, obtained from the Australia Telescope 20 GHz (AT20G) survey, offers the opportunity of an empirical assessment of the completeness and of the reliability of samples extracted from the WMAP 23 GHz map in the same area. Follow-up observations at 20 GHz have yielded accurate flux measurements, allowing us to determine the accuracy of flux and error estimates at the nearby WMAP frequency of 23 GHz. Spectral information is also available, thanks to measurements at 8.6, 4.85 GHz, and, for a subsample, at 95 GHz (Sadler et al. 2008). The lessons learned from the comparison of the results of the analysis of 23 GHz maps with the AT20G data provided an useful guidance for the investigation of WMAP all-sky data also at the other WMAP frequencies. We have limited our study to the first 4 WMAP channels, leaving aside the 94 GHz channel because of the normalization problems discussed by LC07 and GN08.

This paper is organized as follows. In §2 we describe our approach to source detection. The reliability and completeness of the samples of detected sources, and the quality of flux density estimations are discussed, using the BSS data as a benchmark, in §3. In §4 we extend the analysis to the whole $|b| > 5^\circ$ WMAP maps and describe the properties of the NEWPS_5yr catalogue. Finally, in §5, we summarize and briefly discuss our main conclusions.

2 DETECTION TECHNIQUES

The MHW2, that we use in the present study, is the second member of the Mexican Hat Wavelet filter family (González-Nuevo et al. 2006). It is obtained by analytically applying the Laplacian operator twice on the 2D Gaussian function. It operates locally removing simultaneously the large scale variations originated in the diffuse Galactic foregrounds as well as the small scale noise. The scale at which MHW2 operates can be easily optimized so that the signal-to-noise ratio (SNR) of the sources is maximized. This scale is obtained

Sample ID	NEWPS_3yr	WMAP 5-yr NB
Method	non-blind	non-blind
Input positions (for NB)	5 GHz catalogues	NEPWS_3yr_3 σ
Sky coverage	All sky with $ b > 5^\circ$	All sky with $ b > 5^\circ$
SNR > 3 detections	[759, 564, 535, 365]	[712, 585, 537, 312]
SNR > 5 detections	[349, 223, 217, 135]	[366, 262, 246, 122]
median flux density error (mJy)	[182, 219, 214, 251]	[168, 207, 196, 249]
min flux density at SNR > 5 (mJy)	[712, 995, 861, 995]	[754, 888, 861, 950]
Sample ID	WMAP 5-yr SB	WMAP 5-yr IB
Method	simple blind	iterative blind
Sky coverage	All sky with $ b > 5^\circ$	All sky with $ b > 5^\circ$
SNR > 3 detections	[1826, 2279, 3001, 3441]	[1302, 1345, 1575, 1308]
SNR > 5 detections	[454, 304, 285, 155]	[399, 279, 265, 143]
median flux density error (mJy)	[167, 206, 196, 249]	[168, 206, 194, 247]
min flux density at SNR > 5 (mJy)	[695, 874, 831, 1082]	[744, 876, 854, 963]

Table 1. Summary of the main properties of the blind and non-blind (NB) samples discussed in this paper. Values in the square brackets refer respectively to [23, 33, 41, 61] GHz. Note that we have investigated 2 different blind approaches: a ‘simple’ blind (SB) and a ‘iterative’ blind (IB); details are in the text.

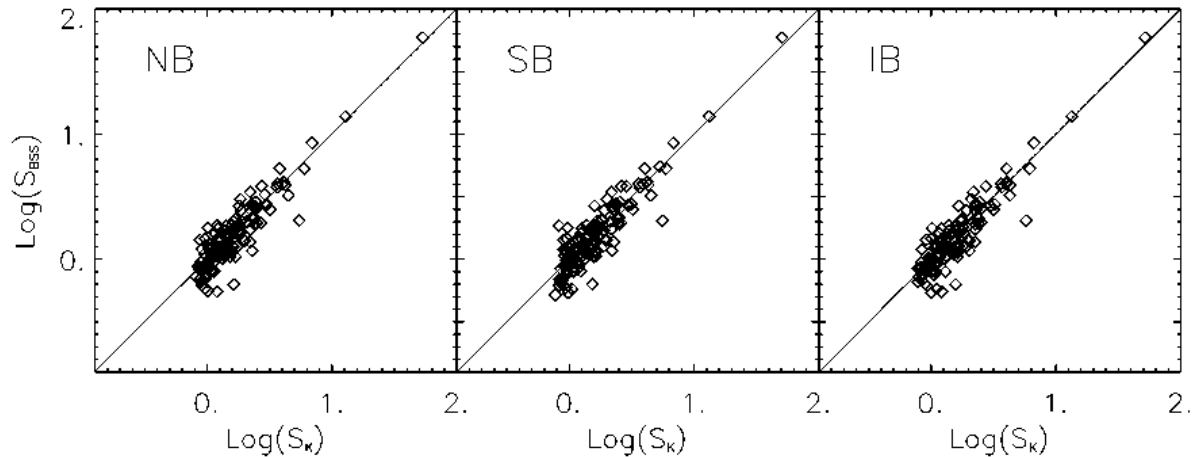


Figure 1. Comparison of flux densities estimated from WMAP maps using each of our 3 methods with the AT20G ones. The agreement is good except for the systematic offset at faint flux densities (see text for further discussion).

numerically in an easy way for any given sky patch. The optimal scale is approximately equal to the beamwidth and generally varies by no more than 10-15 percent except in highly contaminated regions where the variation may be of up to a factor of 2. A comparison of the shapes in the Fourier domain of some matched filters with the corresponding MHW2 at the optimal scale can be found in Lopez-Caniego et al. (2006).

After filtering, the flux is estimated at the position of the maxima. The wavelet can be normalized in such a way that the intensity value at the maxima is equal to the flux of the source. This estimation of the flux is, on average, unbiased. The normalisation of the wavelet is very sensitive to the assumed profile of the signal. In LC07 it was shown how it is possible to go beyond the Gaussian approximation, using the symmetrized radial beam profiles provided by WMAP. In this work we have used the updated 5 year beam profiles throughout the analysis.

In the *simple blind* (SB) approach we look for objects above a given SNR anywhere in the patch. In the *non-blind* (NB) approach, whereby we are looking for WMAP sources at the positions of previously known sources, the patch is chosen so that the source position is right at the center of the patch, and we measure the SNR there. Finally, the *iterative blind* (IB) approach consists in producing, for each source detected with the blind approach, new patches centered at the source positions, and in re-estimating the SNRs.

For this work we have used an end-to-end code that reads in an input parameter file containing the specific characteristics of the maps to be studied, reads in the input map in FITS format, extracts the patches to be analyzed using the tangential plane approximation, finds for each patch the optimal scale of the wavelet, filters each of them with the MHW2 code, produces a list of detections above a given SNR, converts the positions of the detected objects from

the tangent plane to the sphere and, finally, combines the detections into a single output file.

In the input parameter file we specify how to obtain the patches needed for the analysis. In the general case, the code divides and projects the sky into a sufficient number of square patches such that the whole sky is not only fully covered, but also there is a sufficient amount of overlap among the patches to allow cuts of the borders of the image, if needed. The size of the patches in the sky, the pixel size and the amount of overlap among patches are specified in the parameter file. We have used flat projected patches of $14.6^\circ \times 14.6^\circ$, each containing 128×128 pixels. The pixel area is $6.87' \times 6.87'$, corresponding to the HEALPix resolution parameter $N_{\text{side}} = 512$. The patch making routine is part of the CPACK library¹. There is also the option of inputting the list of coordinates of the centers of the patches, corresponding to the known positions of the sources in the cases of the non-blind and of the iterative blind approaches. In the following subsections we will describe in detail how the algorithms work for each approach.

The comparison of fluxes determined from the WMAP 5-year maps with those listed in the NEWPS_3yr catalogue shows good agreement if the same calibration, described in GN08, is applied. In fact, the correction factors to the effective beam areas calculated using the symmetrized beam profiles given by the WMAP team have not changed significantly. Such correction factors are [1.05, 1.086, 1.136, 1.15] at [23, 33, 41, 61] GHz, respectively.

2.1 Simple blind approach

The program reads in the input parameter file and the map in FITS format and calculates the number of flat patches to be extracted and the coordinates of their centers. For our choice of the input parameters ($14.6^\circ \times 14.6^\circ$ patches with 3° overlap) the program extracts 371 flat patches. Next, the code loops over each of them, finding the optimal scale, filtering the maps with the MHW2 at such optimal scale and detecting objects with $\text{SNR} \geq 3$. For each patch a temporary catalogue is obtained, and for each object, the flux at the position of the corresponding peak is estimated. Finally, the temporary catalogues are combined into a final one, removing duplications (in the case of multiple detections of the same source we select the one with the brightest flux, that normally corresponds to the most accurate position).

The rms of the map is obtained via a three step process. First, in order to avoid border effects after filtering, a 15 pixel border around the maps is flagged. Second, all the maxima in the image are identified and a histogram of their values is obtained. Then, the 5 per cent of the brightest maxima are masked, flagging the pixels within a 2 FWHM radius from the position of the maxima. Finally, the rms of the map is calculated excluding the flagged pixels.

2.2 Non-blind approach

In the non-blind approach the patches to be analyzed are centered at the positions of the objects we want to investigate. Since the position of the source is already known, the

goal is to get a good characterization of the noise rms level in its vicinity. The algorithm goes as for the blind approach, with the following differences: i) we have an additional input file, containing the coordinates of the objects; ii) we look for maxima within a circle around the patch center, with 1 FWHM radius; iii) the rms fluctuation level is estimated taking into account only a corona around the patch center, with inner radius of 1 FWHM and an outer radius of 3 FWHM.

In practice, the amplitude of the central maximum (if any) gives an estimate of the source flux, and to compute the rms noise we apply the flagging of pixels at the border, the search of maxima, and the flagging of the 5 per cent brightest, only to the corona. In this way, we try to get a more accurate estimate of the noise in the vicinity of the object of interest, avoiding the contamination by other bright nearby objects.

The application of this approach builds on the work by LC07 who have looked for signals in WMAP 3-year maps at the positions of 2491 sources forming a complete sample mostly selected at 5 GHz. They detected 369 of these sources with $\text{SNR} \geq 5$ in at least one WMAP channel. The detection efficiency is therefore of only 14.8%. The lower noise level in WMAP 5-year data can allow the $\text{SNR} \geq 5$ detection of some, but not many, fainter sources. Thus, we limited our non-blind search to the 933 sources in LC07 associated to $\text{SNR} \geq 3$ peaks in the 3-yr maps.

As discussed below, the AT20G Bright Source Sample (BSS), complete to $S_{20\text{GHz}} = 0.5$ Jy and covering about $1.5 \times 10^4 \text{ deg}^2$, is particularly useful to test the performances of our detection algorithms. Our non-blind approach was first applied to this sample.

2.3 Iterative blind approach

The iterative blind method proceeds in two steps. The first step follows the procedure described in §2.1 and produces as output a list of coordinates that are fed to the non-blind scheme of §2.2. In this way we hoped to combine the potential of the blind detection with the advantages of the local noise estimation of the non-blind method.

2.4 Sampling of the fluctuation field

The choice of the region to be used for estimating the noise level is the best compromise between the conflicting requirements of sufficient statistics and not being affected by variations of the background far from the source position. In fact, we are interested in getting the best estimate of fluctuations at the source position.

This issue may be critical in the cases of the non-blind or iterative blind approaches, since the region where the fluctuation field is sampled is rather limited. However, we have typically 30 independent areas within the sampling region. Using the formalism given by Danese et al. (1980) we find that, for a Gaussian fluctuation field, the uncertainty on the rms fluctuation is [+16%, -12%]. In the case of the simple blind approach we have about 180 independent areas in each region and the uncertainty drops to $\simeq \pm 5\%$.

¹ <http://astro.ic.ac.uk/~mortlock/cpack/>

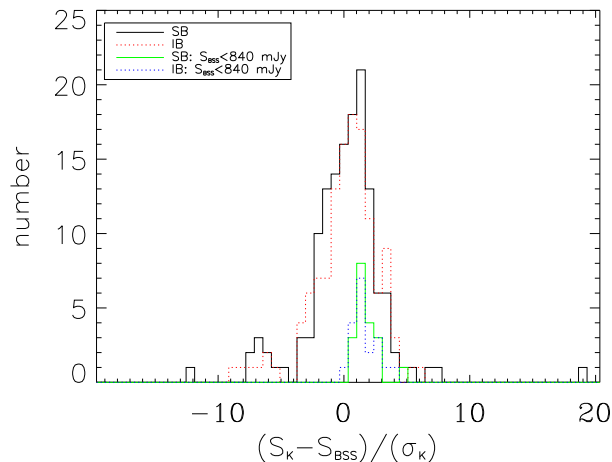


Figure 2. Distribution of the ratio of ‘true’ to estimated errors. S_{BSS} is the ATCA flux density, measured with high SNR, that we assume to be the ‘true’ value. S_{K} and σ_{K} are our flux and error estimates from the WMAP K-band map with the SB and IB methods (see inset). The histograms labeled $S_{\text{BSS}} < 840$ mJy in the inset include only the faint sources whose S_{K} is systematically higher than S_{BSS} (see Fig. 1).

3 BLIND VS NON-BLIND DETECTION: COMPARISON WITH AT20G DATA

The prior knowledge of source coordinates has the obvious advantage that source detection algorithms need to determine only one parameter, i.e. the source flux, while blind detection must deal also with the 2 additional parameters defining the source position, and are exposed to be misled by source blending or small-scale structure in the Galactic emission.

On the other hand, catalogues obtained from a non-blind approach are liable to various possible sources of incompleteness ensuing from the selection that has produced the input catalogue. The latter may have been generated by a survey at a different frequency (generally lower than WMAP’s), with different angular resolution (generally much higher than WMAP’s), carried out at a different epoch. A lower frequency survey may easily miss sources with strongly inverted (i.e. increasing with increasing frequency) spectra. High angular resolution observations (especially the interferometric ones) are insensitive to extended sources, or may pick up only their compact spots, while the sources may be much brighter at the WMAP resolution. Observations at different epochs may catch variable sources in different stages, so that a source that is too faint to be included in the input catalogue may be detected by WMAP, and vice versa.

The AT20G Bright Source Sample (BSS; M08) minimizes the problems mentioned above: i) it has been selected at 20 GHz, i.e. at a frequency close to that of the WMAP K-band channel; ii) the survey has been carried out from 2004 to 2007, i.e. in a period overlapping that of WMAP 5-year maps (obtained averaging over the data collected in 2001-2006). As pointed out by Sadler et al. (2006), on a 1-2 yr time-scale, the general level of variability at 20 GHz has

a median value of 6.9 percent, which is low compared to our uncertainties on flux density estimates. The only completeness problem of the BSS for our analysis is related to the size (2.4’) of the 20 GHz ATCA primary beam. The ensuing incomplete sampling of extended sources will be discussed in the following. Because of its properties, the AT20G BSS constitutes an excellent benchmark against which we may test the performances of blind and non-blind detection techniques applied to the WMAP 23 GHz maps.

Thus, first of all we have performed the Simple Blind (SB) and Iterative Blind (IB) searches on the WMAP 5-yr 23 GHz maps and analyzed the results over the area of the AT20G BSS ($\delta < -15^\circ$), cutting out the Galactic plane region ($|b| < 5^\circ$). This cut removes 26 of the 320 BSS sources. Of the remaining 294 sources, 124 have $S_{\text{BSS}} > 1$ Jy. Next we repeated the search non-blindly, on patches centered at the BSS source positions on the WMAP K-band map. The non-blind technique detected 125 sources (96 with $S_{20\text{GHz}} > 1$ Jy) with $\text{SNR} > 5$; the mean flux density error is of 212 mJy and the minimum detected flux density is of 767 mJy.

The association of peaks in WMAP maps with BSS sources was made adopting a search radius of 21.35’, i.e. equal to $\sigma = \text{FWHM}/2\sqrt{2\ln 2}$ for $\text{FWHM} = 50.277'$. The position of a detection is given by the coordinates of the pixel where a local maximum is found. The median of the distances of the SB detections from the real positions of the sources (given by the AT20G BSS) is 3.7’ (for the iterative blind it is 3.3’), so the positions are typically correct within a pixel for most ($\sim 83\%$) of the objects (the pixel size for the WMAP maps is 6.87’).

The simple blind search recovers 140 BSS sources: 114 are in common with the non-blindly detected sample, but 26 BSS sources have been detected only blindly; 14 BSS sources with $S_{\text{BSS}} > 1$ Jy remain undetected at $\text{SNR} > 5$ level. The iterative blind search, on the other hand, recovers 128 BSS sources: 115 are in common with the non-blindly detected sample, and 13 BSS sources have been detected only blindly; 27 sources remain undetected. Flux estimations are consistent with the BSS measurements, at least for the brightest objects. All the sources with $S_{\text{BSS}} > 1$ Jy undetected by either method show up as local maxima with $\text{SNR} < 5$; most of their fluxes are underestimated, probably because they lie over a negative fluctuation peak. Furthermore the SB and IB searches yielded, respectively, 41 and 30 detections of objects that are not in the BSS.

3.1 Accuracy of flux density and error estimates

A comparison of the flux densities derived from the WMAP maps with those measured by the AT20G survey is shown in Fig. 1. The agreement is generally good, except for the faintest levels ($S_{\text{BSS}} < 840$ mJy) where the WMAP fluxes are systematically higher. Since there are no indications that the faint sources are extended and may therefore be resolved by the AT20G, the discrepancy is likely due to a swelling of the peak at WMAP resolution when the sources happen to be on top of large positive fluctuations due to other components (noise, Galactic emission, CMB). There is no obvious way to identify sources affected by this problem using WMAP data only, and this is another instance of the importance of complementary, higher resolution data. Such

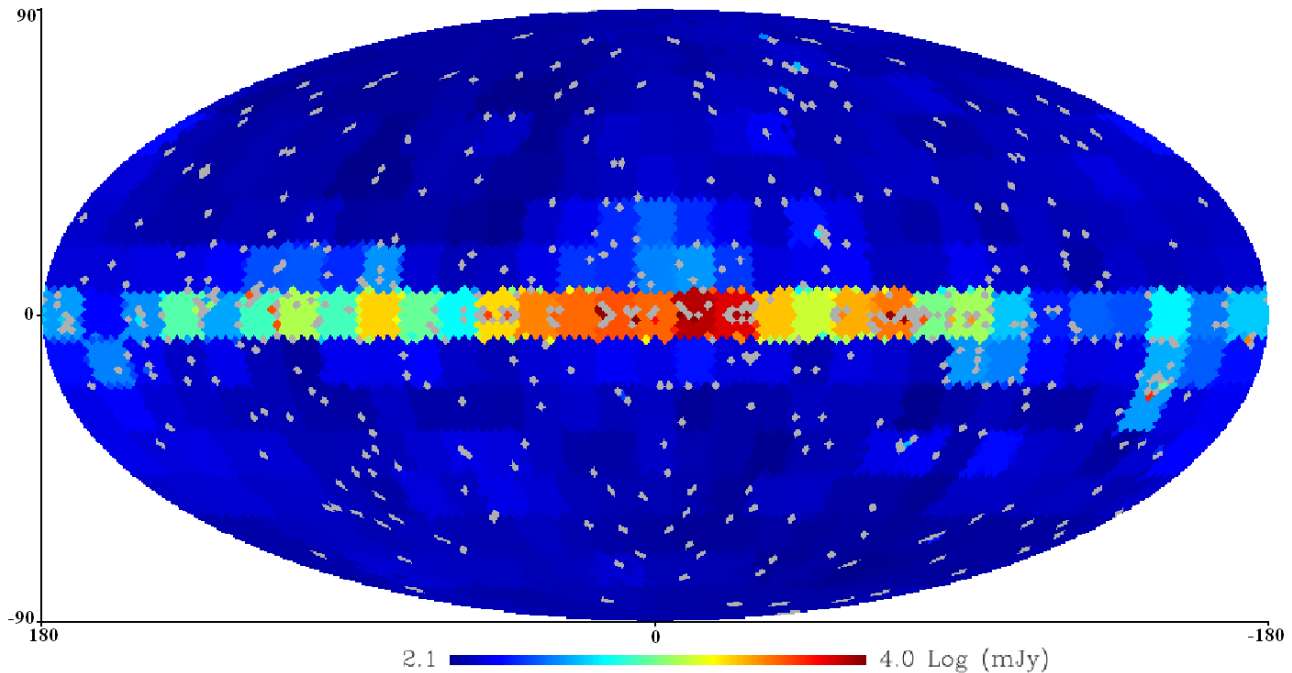


Figure 3. Map (Mollweide projection in Galactic coordinates) of σ_{pixel} for the SB approach at 23 GHz. The pixel area is of $\simeq 3.36 \text{ deg}^2$ (HEALpix pixelization with $N_{\text{side}} = 32$). The patches and the 3° overlaps among detection patches are discernible. Red regions correspond to higher values of noise, darker blue region correspond to lower values (see the colour scale at the bottom of the figure). Grey dots are pixels where no sources are found. A color version of the figure is available on-line.

sources are not found in particularly contaminated regions; on the contrary, the associated noise values are generally rather low.

The comparison of AT20G flux densities, measured with high SNRs, that we assume to be the ‘true’ values, with the flux and error estimates from WMAP maps allow us to assess also the reliability of error estimates. The results are illustrated by Fig. 2. After having removed the sources with $S_{\text{BSS}} < 840 \text{ mJy}$, whose fluxes are systematically overestimated, the median ($S_{\text{K}} - S_{\text{BSS}}$) is 124 mJy for the simple blind and 41 mJy for the iterative blind respectively. Since the distribution is not too different from a Gaussian, the error on the median can be estimated as (Arkin & Colton 1970) $\sigma_{\text{med}} = 1.2533 / [\sum_i (1/\sigma_{\text{K},i})^2]^{1/2} = 18 \text{ mJy}$. An average $\langle (S_{\text{K}} - S_{\text{BSS}}) \rangle \simeq 40 \text{ mJy}$ is expected for an average spectral index $\alpha = 0.3$ ($S_\nu \propto \nu^{-\alpha}$). The simple blind method thus slightly overestimates (by $\lesssim 10\%$) the K-band fluxes, while in the case of the iterative blind method the mean difference with BSS fluxes can be entirely attributed to the small difference in frequency.

After correcting for the small offset, the standard deviation of $(S_{\text{K}} - S_{\text{BSS}})/\sigma_{\text{K}}$ is 2.4 for the SB and 2.0 for the IB sample; more than 93% of the sources lie within 3 standard deviations from the mean (both including and removing the sources with $S_{\text{BSS}} < 840 \text{ mJy}$). The fact that the rms differences between the BSS fluxes, S_{BSS} , and our estimates from WMAP K-band maps, S_{K} , are about twice the average σ_{K} is not surprising. As pointed out by LC07, by applying the optimum filters to WMAP temperature maps we get an average amplification of the SNR, or equivalently,

a damping of the fluctuation level by a substantial factor. In other words, the fluctuation level in the original map due to a combination of anisotropies in the CMB and foreground emissions plus noise, that determines the true uncertainty on the flux estimate, is substantially higher than that in the filtered map, used to estimate σ_{K} . The ratio of the two noise levels is a measure of the detection efficiency of the adopted algorithm.

3.2 Reliability of detections

As mentioned above, the SB and the IB approaches yielded a number of detections without a BSS counterpart. To check whether these sources are real we have looked for counterparts in the NASA Extragalactic Database (NED²). Of the 41 non-BSS detections of the SB search, 15 were found to be extragalactic and 9 Galactic sources, while of the 30 IB non-BSS sources 12 were found to be extragalactic, and 4 Galactic. The BSS is biased against Galactic sources, mostly because they are generally extended; in fact no known Galactic source is included in it. It has also completely missed the very extended extragalactic source Fornax A (detected in WMAP maps). All the other extragalactic sources that were detected by our blind techniques and have counterparts in the NED were also detected by the AT20G survey, but below the BSS flux density threshold. Since accurate estimates of the total flux density of the known extended sources in the area (except for Fornax A) have been obtained with ATCA

² <http://nedwww.ipac.caltech.edu/>

observations in the mosaic mode, the discrepancy cannot be attributed to resolution effects, and in fact there is no indication that the sources in question are extended. We therefore conclude that the K-band fluxes are overestimated, probably because these sources happen to be on top of positive fluctuations of noise and/or Galactic and/or CMB signals within the WMAP beam.

The 17 SB objects (or the 14 IB ones) that do not have a consistent counterpart in the NED may be knots in the Galactic emission, as suggested by the fact that 14 (or 9 for the IB) of these sources are at $|b| < 20^\circ$. To better characterize the sky regions more liable to the occurrence of spurious detections we have produced a 23 GHz noise map (Fig. 3) with pixels size of $\simeq 3.36 \text{ deg}^2$, corresponding to the HEALPix $N_{\text{side}} = 32$ (the size of patches discussed above corresponds to $N_{\text{side}} = 4$). Figure 4 shows that a $\pm 10^\circ$ Galactic cut removes almost all the most contaminated pixels, but also some clean regions. The $\pm 5^\circ$ Galactic cut that we have used so far seems to be a better compromise between removing very contaminated regions and saving clean ones. However, the selection could be improved by selecting a mask for contaminated regions exploiting the information given by the noise map itself.

As illustrated by Fig. 5, most (but not all) of the objects that do not have a consistent counterpart in the NED lie in regions where the noise level is relatively high. Dropping areas with $\sigma_{\text{pixel}} \geq 1.5\sigma_{\text{median}} = 253 \text{ mJy}$ at 23 GHz, where $\sigma_{\text{median}} = 169 \text{ mJy}$ is the median noise level for all pixels at $|b| > 5^\circ$, removes 17 SB sources and 11 IB ones; 9 of the SB and 5 of the IB sources removed are doubtful. We thus approximately halve the number of possibly spurious SB sources at the cost of losing $\simeq 7\%$ of the sky region with $|b| > 5^\circ$ covered by the AT20G BSS (the remaining area amounts to 3.77 sr). This criterion is a good trade-off between completeness and reliability of the sample, and we will adopt it for the all-sky analysis. As for the reliability, only 8 SB sources and 9 IB sources detected in regions with $\sigma_{\text{pixel}} < 1.5\sigma_{\text{median}}$ do not have a consistent low-frequency counterpart. If they are all spurious, the sample reliability is 95.5% for the SB and 94.3% for the IB.

3.3 Completeness

The inhomogeneity of the fluctuation field translates into a spatially varying effective depth of the survey. Correspondingly, the effective area to be used to derive the source counts decreases with decreasing flux limit. This is illustrated by Fig. 3 showing the map of the noise within the $\simeq 3.36 \text{ deg}^2$ pixels (σ_{pixel}). Note that σ_{pixel} is approximately the same in all the pixels within a detection patch and vary on the edge of it because of the overlap among patches. The regions of both higher (Galactic plane, Orion region, Ophiuchus complex, LMC, ...) and lower (Ecliptic pole regions) fluctuation levels can be clearly discerned.

Our final sample is almost 100% complete over the unmasked BSS area above 2 Jy (only 1 source with $S_{\text{BSS}} = 2.06 \text{ Jy}$ is detected with $\text{SNR} < 5$ level). The completeness above 1 Jy of the SB sample is 89%, and that of the IB is 80%. It increases respectively to 91% and 82% including the non-blind detections.

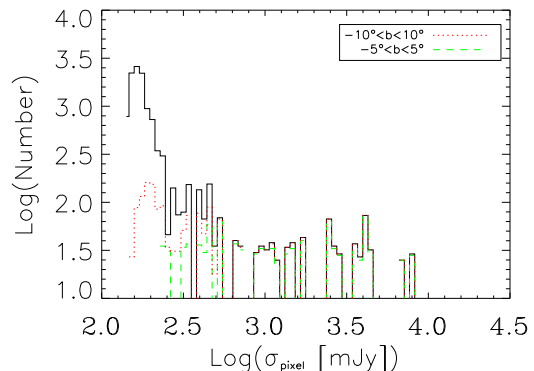


Figure 4. Distribution of the values of σ_{pixel} (pixels size of $\simeq 3.36 \text{ deg}^2$) over the whole sky (solid line), the region within $|b| < 10^\circ$ (dotted line), and the region within $|b| < 5^\circ$ (dashed line).

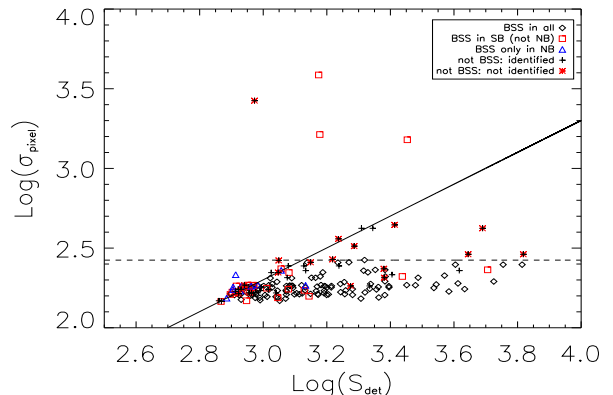


Figure 5. Noise at the source position versus flux density at 23 GHz estimated with the SB approach. The dashed line corresponds to 1.5 times the median noise for the pixels at $|b| > 5^\circ$. The solid line corresponds to $S_K = 5\sigma_{\text{pixel}}$. 11 sources have $S_K < 5\sigma_{\text{pixel}}$ and correspond to $\text{SNR} > 5$ detections in highly contaminated pixels ($\sigma_{\text{pixel}} \gg \sigma_K$; remember that σ_K is computed over a much larger area than σ_{pixel}).

3.4 Simple blind vs iterative blind approach

The performances of SB and IB methods are similar. The SB method recovers with $\text{SNR} > 5$ more sources also in highly contaminated regions, but in those regions the fraction of spurious detections is higher. Hence, choosing among the two approaches amounts to choosing among slightly higher completeness (SB) and slightly higher reliability (IB). On the whole, there is no clear advantage in adopting the more complex IB approach, and we will no longer consider it.

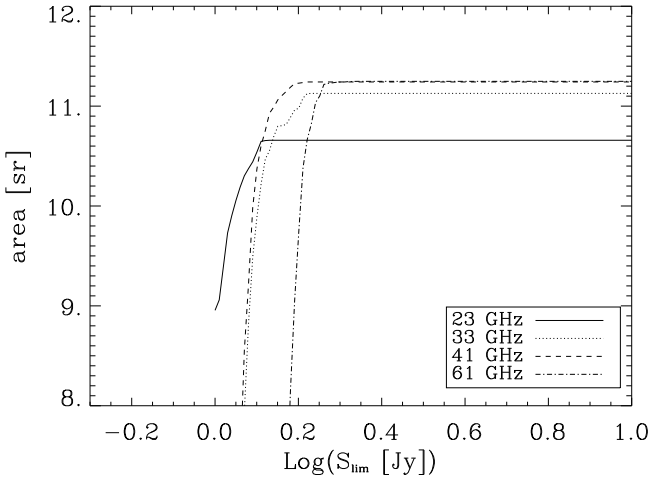
Table 2. Summary of the properties of the NEWPS_5yr_5 σ catalogue. Areas with $\sigma_{\text{pixel}} > 1.5\sigma_{\text{median}}$ have been left aside.

	Total	23 GHz	33 GHz	41 GHz	61 GHz
σ_{median} (mJy)		169	206	196	250
Area selected [sr]		10.66	11.12	11.24	11.25
Simple blind detections		405	281	275	147
Additional non-blind detections		28	26	26	14
Total number of objects $ b > 5^\circ$	516	433	307	301	161
Total number of objects with $5 < b < 10^\circ$	51				
Total number of objects within the LMC boundaries	10				
Total number of identified Galactic objects	27	11	14	21	10
Total number of identified extragalactic objects	457	406	281	268	147
Total number of objects missing a consistent counterpart	32	16	12	12	4
Number of sources in WMAP_5yr	352				
Number of sources only in WMAP_5yr	36				

Table 3. Sample of the NEWPS_5yr_5 σ catalogue. ‘ r_{xx} ’ is the ratio between the σ_{pixel} at the source and the median σ_{median} in the WMAP band at xx GHz. The full table is available on the webpage <http://max.ifca.unican.es/caniego/NEWPS/>

#	RA	δ	l	b	S ₂₃	S ₃₃	S ₄₁	S ₆₁	σ_{23}	σ_{33}	σ_{41}	σ_{61}	r ₂₃	r ₃₃	r ₄₁	r ₆₁	flags	z	Id.
1	0.9780	68.6173	118.6020	6.1460	.	.	.2141	.	.	.250	.	.	.135	...BG..u			
2	1.0589	-47.6401	324.0430	-67.5070	947	967	.	.159	174	.	.095	0.91	.	BN....We	.				PKS 0002-478
3	1.5432	-6.3719	93.4960	-66.6210	2523	2672	2604	2328	170	224	200	257	1.01	1.04	1.01	1.02	BBBB..We	0.3470	PKS 0003-066
4	2.6655	11.0522	107.0640	-50.5590	1253	1235	1274	.	.163	217	198	.	.098	1.03	1.02	.	BBB...We	0.0893	PKS J0010+1058
5	3.2328	-39.9448	332.4160	-74.9010	1182	1385	970	1144	153	190	185	227	0.91	0.92	0.94	..95	BBBN..We	.	PKS 0010-401
6	4.8773	20.2997	112.8470	-41.9460	974	.	.	.165	.	.	.098	.	.	B....We	.				PKS 0017+200
7	4.9167	26.0203	114.0680	-36.3040	1140	.	.	.163	.	.	.097	.	.	B....We	.	0.2840			PKS J0019+2602
8	4.9285	73.5179	120.6480	10.7870	.	.1469	.	.	.254	.	.	.133	..N....e			1.7810			GB6 J0019+7327
9	6.5216	-26.1011	41.7750	-84.2420	904	.	.	.157	.	.	.094	.	.	B....We	.	0.3220			PKS 0023-26
10	6.6014	-35.1350	335.1410	-80.3720	1299	1190	1505	1443	153	190	185	238	0.92	0.95	0.94	0.95	BBBB..We	.	PMN J0026-3512

Note: Coordinates in degrees, flux densities in mJy. Flags column: the first four characters indicate for each WMAP channel used whether the flux density was estimated with the blind (B) or the non-blind (N) method; the fifth character identifies sources at $|b| < 10^\circ$ (G); the sixth character indicates sources within 5° from the center of the Magellanic Cloud (L); a ‘W’ as the seventh character stands for sources in the WMAP_5yr catalogue; the eighth character gives the source identification: ‘g’ is for Galactic, ‘e’ is for extragalactic sources, and ‘u’ is for sources that miss a consistent counterpart.

**Figure 6.** Effective area as a function of the flux limit $S_{\text{lim}} = 5\sigma_{\text{pixel}}$, for the simple blind method.

4 BLIND AND NON-BLIND SOURCE DETECTION ON ALL-SKY WMAP 5-YR MAPS.

The analysis of the BSS sample, described above, provides useful guidance for the analysis of all-sky WMAP 5-yr maps at 23, 33, 41 and 61 GHz, to produce the NEWPS_5yr catalogue. For each map we have performed the following steps.

- We have carried out a simple blind search over the whole sky.
- We have produced maps of the mean noise values per pixel corresponding to $N_{\text{side}} = 32$, σ_{pixel} , and computed the median of such values for $|b| < 5^\circ$, σ_{median} .
- We have masked all the pixels with noise level $> 1.5\sigma_{\text{median}}$, which, as found in the previous analysis, contain a large fraction of the doubtful detections.
- We have taken all the sources with $\text{SNR} > 5$ outside the masked area as true detections.
- By counting the number of pixels for which $5\sigma_{\text{pixel}}$ is smaller than any given flux density limit, S_{lim} , we obtain the effective area, as a function of S_{lim} , to be used to estimate the differential source counts (see Fig. 6). The decrease of the effective area with decreasing flux density is consistent with the decrease of the fraction of detected BSS sources

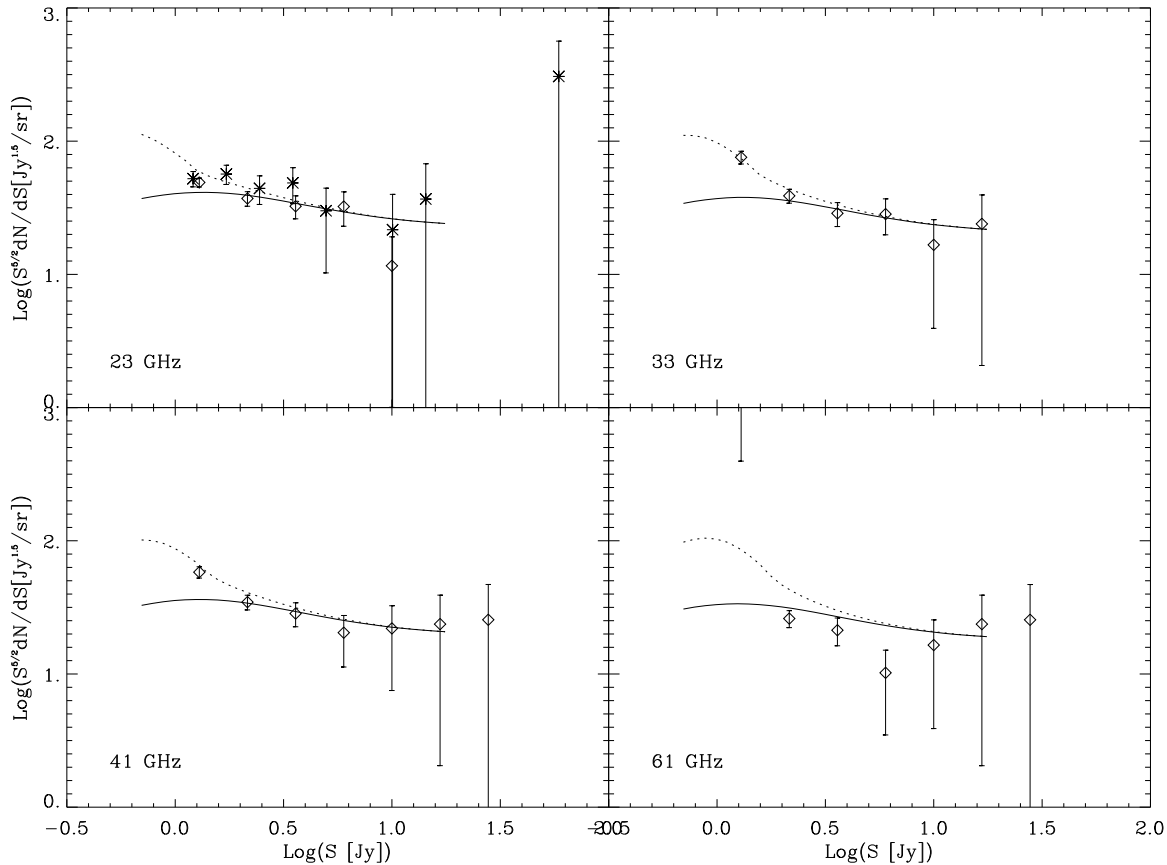


Figure 7. Differential WMAP counts, normalized to $S_{\text{Jy}}^{-2.5}$, estimated from the WMAP data (diamonds). The 23 GHz counts are compared with the ATCA 20 GHz ones (asterisks). The solid lines show the predictions of the model by De Zotti et al. (2005). The dotted lines illustrate the effect of the Eddington bias by showing the model counts convolved with a Gaussian error distribution with $\sigma = 0.34, 0.42, 0.4, 0.5$ Jy at 23, 33, 41, and 61 GHz, respectively. The value of σ at 23 GHz was obtained by comparison with the BSS measurements. At higher frequencies we assumed that the true errors on flux measurements are twice the median errors yielded by the simple blind approach, as found at 23 GHz. The convolution has been computed integrating down to a minimum flux equal to $S/10$.

reported in §3.3. The maximum effective area is given, for each WMAP channel, in the second row of Table 2.

Next, we carried out a non-blind search on the 5-yr WMAP maps at the positions of sources in the NEWPS_3yr_3 σ sample (see §1). This search has produced 28 additional SNR > 5 detections at 23 GHz.

The main properties of the NEWPS_5yr_5 σ catalogue, including SNR > 5 detections obtained with both the blind and the non-blind approach, are summarized in Table 2. The sample totals 516 sources detected in the regions where $\sigma_{\text{pixel}} \leq 1.5\sigma_{\text{median}}$. A search in the NED yielded 457 identifications with extragalactic sources and 27 identifications with Galactic objects. Only for 32 objects no consistent counterparts were found (5 of them are clearly in the region of the nebula NGC 1499). Even if they are all spurious, the reliability of our sample is of 93.8%, close to that found from the comparison with the BSS sample.

Of the 388 WMAP_5yr sources in the sky region covered by the NEWPS_5yr_5 σ catalogue, 352 have been recovered. All the other 36 have detections below our SNR = 5 threshold. On the other hand, the NEWPS_5yr_5 σ catalogue contains 164 objects not in WMAP_5yr. 31 of the new sources

do not have consistent counterparts in low frequency catalogues and may therefore be spurious.

Of the 64 sources detected by Chen & Wright (2008) in the 3-yr catalogue, 50 are in our NEWPS_3yr at 61 GHz. All the 64 objects have been recovered in the present analysis, but 6 of them are below the SNR = 5 threshold. Our NEWPS_5yr_5 σ catalogue also includes all the sources detected by Nie & Zhang (2007) outside the LMC region and at $|b| > 5^\circ$, not present in the 3-year WMAP catalogue.

The first lines of the NEWPS_5yr_5 σ catalogue are shown in Table 3. The full catalogue, the catalogue of the 3 SNR detections, and the noise maps are available on the web page <http://max.ifca.unican.es/caniego/NEWPS/>.

The counts of WMAP sources for each channel are presented in Table 4 and in Fig. 7. They have been estimated calculating the effective area over which each source could have been detected (Fig. 6) and summing the inverse areas in the flux density bin of interest (Katgert et al. 1973). Error estimates use the approximation formulae for a Poisson statistics recommended by Gehrels (1986), with an effective number of sources

Table 4. The differential normalized source counts ($\log(S^{5/2}dN/dS[\text{Jy}^{1.5}/\text{sr}])$) of WMAP sources for each channel. No correction for the Eddington bias has been applied (see the text and the caption of Fig. 7 for details).

log S [Jy]	23 GHz	33 GHz	41 GHz	61 GHz
0.1	1.69 ^{+0.03} _{-0.03}	1.87 ^{+0.04} _{-0.05}	1.77 ^{0.04} _{-0.04}	3.51 ^{0.27} _{-0.91}
0.3	1.57 ^{+0.05} _{-0.06}	1.59 ^{+0.05} _{-0.06}	1.54 ^{0.05} _{-0.06}	1.42 ^{0.06} _{-0.07}
0.5	1.51 ^{+0.08} _{-0.09}	1.46 ^{+0.08} _{-0.10}	1.45 ^{0.08} _{-0.10}	1.33 ^{0.09} _{-0.12}
0.8	1.51 ^{+0.11} _{-0.15}	1.45 ^{+0.11} _{-0.16}	1.31 ^{0.13} _{-0.26}	1.01 ^{0.17} _{-0.47}
1.0	1.06 ^{+0.22} _{-1.06}	1.22 ^{+0.19} _{-0.63}	1.34 ^{0.17} _{-0.47}	1.22 ^{0.19} _{-0.63}
1.2		1.38 ^{+0.22} _{-1.06}	1.37 ^{0.22} _{-1.06}	1.37 ^{0.22} _{-1.06}
1.4			1.41 ^{0.26} _{-11.4}	1.41 ^{0.27} _{-11.4}

$$n_{\text{eff}} = \frac{\left(\sum_i (1/A_i)\right)^2}{\sum_i (1/A_i)^2}. \quad (1)$$

As expected, the counts are systematically overestimated at the faintest flux densities, by effect of the Eddington bias. At 23 GHz, the De Zotti et al. (2005) model suggests that the overestimate is of about 15% at 2 Jy, and rapidly increases with decreasing flux (it is $\simeq 30\%$ at 1.5 Jy, and reaches a factor of almost 2 at 1 Jy).

5 DISCUSSION AND CONCLUSIONS

We have analyzed the efficiency in source detection and flux density estimation of *blind* and *non-blind* detection techniques based on the MHW2 filter applied to the WMAP 5-year maps. Comparing with a complete sample of radio sources, the AT20G Bright Source Sample (BSS; M08), selected at 20 GHz, close to the lowest WMAP frequency, with very high signal-to-noise flux measurements, and almost contemporary to the WMAP survey, we estimated the completeness, the reliability, and the accuracy of flux density and error estimates for the samples detected with the two approaches.

We found that flux density estimates are essentially unbiased except at the faintest flux densities ($S_{\text{BSS}} < 840 \text{ mJy}$), where the fraction of the source intensity peaks amplified by positive fluctuations due to other components (Galaxy, CMB, noise) within the WMAP beam becomes substantial and the source counts are correspondingly overestimated. This is a manifestation of the Eddington bias, enhanced by the fact that the true errors on flux density estimates turn out to be about a factor of 2 higher than the errors estimated by our procedure (see §3.1). The difference is due to the filtering of the maps that increases the signal-to-noise ratio by smoothing the fluctuation field. No clear-cut criterion capable of identifying sources affected by this problem using only WMAP data was found. However, coupling the estimate of the true uncertainties on source fluxes, obtained by comparison with the high signal-to-noise ATCA 20 GHz measurements, with information on counts below the WMAP detection limit we may estimate the corresponding corrections on source counts. Using the De Zotti et al. (2005) model, that incorporates the information on counts provided by the AT20G (M08; Ricci et al. 2004) and 9C (Waldrum et al. 2003) surveys at nearby frequencies we estimate that, in the K-band, the counts have to be cor-

rected downward by about 15% at 2 Jy, and by a factor of almost 2 at 1 Jy.

At higher flux densities most (17 out of 19) of probably spurious detections are at relatively low Galactic latitudes ($|b| < 20^\circ$), suggesting that the observed intensity peaks are largely due to small scale structure in the Galactic emission. Excluding the areas where the rms fluctuations are more than 50% higher than the $|b| > 5^\circ$ median approximately halves the number of dubious candidates, at a modest cost ($\simeq 7\text{--}10\%$) in terms of useful area. If all dubious sources are spurious, the reliability of the sample is 95.5%.

The blind detection approach applied to the all-sky WMAP maps, excluding the Galactic plane region ($|b| < 5^\circ$) and the areas where the rms fluctuations are more than 50% higher than the median value at $|b| < 5^\circ$, has found 488 candidate sources with $\text{SNR} > 5$ in at least one WMAP channel. The non-blind approach has added 28 further objects, raising the total to 516, to be compared with the 388 sources listed in the WMAP 5-yr catalog (Wright et al. 2008). Almost all (484) sources in our sample were previously catalogued extragalactic (457) or Galactic (27) objects. The remaining 32 candidate sources do not have counterparts in lower frequency all sky surveys with comparable flux densities and may therefore be just high peaks in the distribution of other components present in the maps. If they are all spurious, the reliability of the sample is 93.8%.

ACKNOWLEDGEMENTS

Partial financial support for this research has been provided to MM, JGN, and GDZ by the Italian ASI (contracts Planck LFI Activity of Phase E2 and I/016/07/0 ‘COFIS’) and MUR, and to JLS by the Spanish MEC. MLC acknowledges a postdoctoral fellowship from the Spanish MEC. JGN acknowledges a postdoctoral position at the SISSA-ISAS (Trieste). JLS thanks the CNR ISTI in Pisa for their hospitality during his sabbatical leave. This research has made use of the NASA/IPAC Extragalactic Database (NED) which is operated by the Jet Propulsion Laboratory, California Institute of Technology, under contract with the National Aeronautics and Space Administration. Some of the results in this paper have been derived using the HEALPix (Górski et al., 2005) package. Part of this analysis has been carried out using Grid infrastructure in the framework of the project EGEE (reference FP7 INFISO-RI 222667).

REFERENCES

- Argüeso F., González-Nuevo J., Toffolatti L., 2003, ApJ, 598, 86
- Arkin H., Colton R.R., 1970, Statistical Methods, Barnes & Noble Books, Harper & Row Pub., New York
- Bennett C. L., et al., 2003, ApJS, 148, 97
- Chen X., Wright E. L., 2007, arXiv, 712, arXiv:0712.3594
- Condon J. J., Cotton W. D., Greisen E. W., Yin Q. F., Perley R. A., Taylor G. B., Broderick J. J., 1998, AJ, 115, 1693
- Danese L., de Zotti G., di Tullio G., 1980, A&A, 82, 322
- De Zotti G., Ricci R., Mesa D., Silva L., Mazzotta P., Toffolatti L., González-Nuevo J., 2005, A&A, 431, 893

- De Zotti G., Toffolatti L., Argüeso F., Davies R. D., Mazzotta P., Partridge R. B., Smoot G. F., Vittorio N., 1999, AIPC, 476, 204
- Eddington A. S., 1913, MNRAS, 73, 359
- Gehrels N., 1986, ApJ, 303, 336
- González-Nuevo J., Argüeso F., López-Caniego M., Toffolatti L., Sanz J. L., Vielva P., Herranz D., 2006, MNRAS, 369, 1603
- González-Nuevo J., Massardi M., Argüeso F., Herranz D., Toffolatti L., Sanz J. L., López-Caniego M., de Zotti G., 2008, MNRAS, 384, 711 (GN08)
- Górski K. M., Hivon E., Banday A. J., Wandelt B. D., Hansen F. K., Reinecke M., Bartelmann M., 2005, ApJ, 622, 759
- Gregory P. C., Scott W. K., Douglas K., Condon J. J., 1996, ApJS, 103, 427
- Griffith M. R., Wright A. E., 1993, AJ, 105, 1666
- Griffith M. R., Wright A. E., Burke B. F., Ekers R. D., 1995, ApJS, 97, 347
- Hinshaw G., et al., 2007, ApJS, 170, 288
- Hogg D. W., Turner E. L., 1998, PASP, 110, 727
- Katgert P., Katgert-Merkelijn J. K., Le Poole R. S., van der Laan H., 1973, A&A, 23, 171
- Leach S.M., et al., 2008, A&A, submitted, arXiv:0805.0269
- López-Caniego M., Herranz D., González-Nuevo J., Sanz J. L., Barreiro R. B., Vielva P., Argüeso F., Toffolatti L., 2006, MNRAS, 370, 2047
- López-Caniego M., González-Nuevo J., Herranz D., Massardi M., Sanz J. L., De Zotti G., Toffolatti L., Argüeso F., 2007, ApJS, 170, 108 (LC07)
- Massardi M., et al., 2008, MNRAS, 384, 775 (M08)
- Mauch T., Murphy T., Buttery H. J., Curran J., Hunstead R. W., Piestrzynski B., Robertson J. G., Sadler E. M., 2003, MNRAS, 342, 1117
- Mauch T., Murphy T., Buttery H. J., Curran J., Hunstead R. W., Piestrzynski B., Robertson J. G., Sadler E. M., 2007, yCat, 8081, 0
- Murdoch H. S., Crawford D. F., Jauncey D. L., 1973, ApJ, 183, 1
- Nie J.-Y., Zhang S.-N., 2007, ChJAA, 7, 199
- Ricci R., et al., 2004, MNRAS, 354, 305
- Sadler E. M., et al., 2006, MNRAS, 371, 898
- Sadler E. M., Ricci R., Ekers R. D., Sault R. J., Jackson C. A., de Zotti G., 2008, MNRAS, 385, 1656
- Toffolatti L., De Zotti G., Argüeso F., Burigana C., 1999, ASPC, 181, 153
- Waldram E. M., Pooley G. G., Grainge K. J. B., Jones M. E., Saunders R. D. E., Scott P. F., Taylor A. C., 2003, MNRAS, 342, 915
- Wright A. E., Griffith M. R., Burke B. F., Ekers R. D., 1994, ApJS, 91, 111
- Wright A. E., Griffith M. R., Hunt A. J., Troup E., Burke B. F., Ekers R. D., 1996, ApJS, 103, 145
- Wright E. L., et al., 2008, arXiv, 803, arXiv:0803.0577